# Application of unimolecular reaction rate theory for highly flexible transition states to the dissociation of $CH_2CO$ into $CH_2$ and CO. II. Photofragment excitation spectra for vibrationally-excited fragments

Stephen J. Klippenstein[a)]
*Department of Chemistry and Biochemistry, University of Colorado, Boulder, Colorado 80309-0215*

R. A. Marcus
*Arthur Amos Noyes Laboratory of Chemical Physics, California Institute of Technology, Pasadena, California 91125*[b)]

(Received 27 December 1989; accepted 7 May 1990)

Results on vibrationally-excited ketene photofragment excitation (PHOFEX) spectra of Moore and co-workers are interpreted in terms of a previously described variational implementation of Rice–Ramsberger–Kassel–Marcus (RRKM) theory. At subvibrational excitations, the predictions of this theory reduce to those of phase space theory (PST). However, for excess energies just above the threshold of excitation of a particular vibrational mode of the products, the present theory predicts a significantly greater probability for vibrational excitation, compared with PST, in closer agreement with the experimental results, and predicts an energy dependence of the PHOFEX spectrum that is closer to the observed one. A key feature, to which the present calculations lead, is a two-transition state (TS) description for each vibrational excitation of the products, the PST TS region dominating at the threshold for that excitation and an inner TS region dominating at somewhat higher ($\sim 200\ cm^{-1}$) energies. The behavior contrasts partly with that of the unimolecular dissociation rate constant $k_{EJ}$ (except at the threshold for $k_{EJ}$), because of the different focus of the two types of measurements. The theory provides a consistent interpretation of both properties.

## I. INTRODUCTION

In Part I, unimolecular dissociation rates of vibrationally energetic $^1CH_2CO$ molecules as a function of their excess energy[1] were calculated using variational Rice–Ramsberger–Kassel–Marcus (RRKM) theory. In the comparison with the experimental results of Zewail and co-workers,[2] there was good agreement of the two, much improved over the rates calculated from phase space theory.[3] Phase space theory (PST) serves as a very useful benchmark model, by showing what can be expected for the completely "loose" transition state (TS), i.e., for a TS in which the separating fragments rotate freely. The RRKM-based calculation allows for their hindered rotations, which may occur in the transition state. In PST,[4] in the present variational RRKM theory,[5,6] and in other treatments[7] of the rates, the position of the TS in a unimolecular dissociation typically moves to shorter fragment–fragment separation distances with increasing temperature $T$ or energy $E$. Correspondingly, because of an enhanced hindrance of fragment rotations at smaller separation distances, the difference between the results of PST and variational RRKM calculations usually increases when $E$ or $T$ is increased.

In Part I it was also noted that the photofragment excitation (PHOFEX) spectra predicted from an RRKM-based theory for the quantum state distribution of the separated fragments[8] reduce to those predicted from PST when the excess energy is insufficient to cause vibrational excitation of the reaction products. PST for the subvibrational excitation spectra was shown previously by Moore and co-workers to agree with their PHOFEX data.[9,10] However, at energies somewhat in excess of the threshold for vibrational excitation of the products, it was calculated in Part I that an appreciable difference between quantum product state distributions determined from PST and the RRKM-based theory could occur. The results of the corresponding theoretical calculations for the PHOFEX spectra are given in the present paper and compared with experimental results[11] of Moore and co-workers. Since the comparison of the RRKM-based PHOFEX spectra at subvibrational energies[9,10] with the experimental data reduces, as noted in Part I, to the corresponding comparison of PST with experiment (aside from a separate consideration of the singlet/triplet yield),[1] they are not considered further here.

Other methods for determining product state distributions, such as the adiabatic channel model[12] and the separate statistical ensembles method,[13] have been described elsewhere. However, the focus of the present article is a comparison of the PHOFEX spectra predicted by PST and RRKM theories, both with each other and with the experimental data. The theory of the products' quantum state distribution used here is described in Sec. II A, the application to PHOFEX spectra in II B, and results and discussion are given in Sec. III. The main finding is given in a summary, Sec. IV.

[a)] Present address: Chemistry Department, Case Western Reserve University, Cleveland, OH 44106.
[b)] Contribution No. 8095.

 0021-9606/90/162418-07$03.00 

## II. THEORY

### A. Quantum state distributions

We first recall several aspects of the variational RRKM-based calculations for the reaction rates[1,5,6] and for the quantum state distribution of the products[1,6,8] of dissociations occurring at a given total energy $E$. In these calculations, an approximate separation of variables is made in the exit channel region into the "conserved" modes and the "transitional" modes.[1,5,6] The conserved modes are those that retain their vibrational nature in the evolution from reactants to products, while the transitional modes consist of all remaining motions, including rocking vibrations, that become free rotations. In the calculation of the distribution of the quantum states of the products, a dynamical assumption is made for the evolution of each of the two types of modes along the exit channel: the conserved modes are treated adiabatically in the vicinity of and after the transition state region(s), while the transitional modes are treated nonadiabatically in that region, as described in Refs. 4(a) and 8 and, for completeness, at the end of the present subsection.

A key quantity in the calculation of the products' quantum state distribution is $N^{\dagger}_{EJ,i}$, the number of quantum states having an energy equal to or less than $E$, for the particular state $i$ of the conserved modes at its TS and for a given total angular momentum quantum number $J$. The quantity $N^{\dagger}_{EJ,i}$ is determined for each $E$ by considering an $N_{EJ,i}(R)$ at each value of the reaction coordinate $R$. Note that $N^{\dagger}_{EJ,i}$, and therefore the position of the TS, occurs at the minimum of $N_{EJ,i}(R)$:

$$N^{\dagger}_{EJ,i} = \text{Min}\, N_{EJ,i}(R) \quad (R_0 \leqslant R \leqslant \infty), \tag{1}$$

where $R_0$ is some minimum $R$ considered, and an expression for $N_{EJ,i}(R)$ is given in Ref. 14. In the present calculation, $R_0$ is taken to be 2.4 Å. We note that this variational determination of the $N^{\dagger}_{EJ,i}$ for each $i$ corresponds to determining a separate transition state for each conserved mode state $i$. In Eq. (1), the energy and angular momentum are conserved during the dissociation of the molecule. The effect of conservation of nuclear spin and parity with respect to inversion was considered in the Appendix of Part I. In the present calculations of the PHOFEX spectra, the latter two quantities are also assumed to be conserved, as discussed in Ref. 9.

Sometimes, two local minima for the $N_{EJ,i}(R)$ in Eq. (1) may occur, with important consequences, as seen below, for the interpretation of PHOFEX spectra. As noted in Part I, since each state $i$ of the conserved modes is treated adiabatically in the region between the two minima, no transition between two different states of the conserved modes need be considered there. In this case, the appropriate $N^{\dagger}$ is $N^{eff}_{EJ,i}$, given by[1]

$$\frac{1}{N^{eff}_{EJ,i}} = \frac{1}{N^{\dagger 1}_{EJ,i}} + \frac{1}{N^{\dagger 2}_{EJ,i}} - \frac{1}{N^{\max}_{EJ,i}}, \tag{2}$$

where $N^{\dagger 1}_{EJ,i}$ and $N^{\dagger 2}_{EJ,i}$ represent the number of states at the two minima in the flux, and $N^{\max}_{EJ,i}$ represents the maximum in the number of states in between these two minima. It may be noted that when $N^{\dagger 1}_{EJ,i}$ and $N^{\dagger 2}_{EJ,i}$ differ appreciably, Eq. (2) reduces to Eq. (1). This form for $N^{eff}$ has been used previously in calculations of rates.[6,14,15] Here, we give what appears to be the first detailed example of its use for specific quantum state distributions.

Equations (1) and (2) are used below in two alternative calculations of the product vibrational distribution and for the comparison with the experimental results. The method used here and the parameters employed to calculate these numbers of states have been described in Part I, and so only a few further details are described below.[16,17] The potential energy surface described in Part I was also used here. This surface represents the C = C bonding interaction in terms of a Varshni potential and the fragment–fragment van der Waals interactions in terms of Lennard–Jones 6–12 potentials.

The number of states at the outer minimum $N^{\dagger 2}_{EJ,i}$ was calculated with quantum PST, and so we label it below as $N^{PST}_{EJ,i}$: it represents in the present case the number of PST states having a specific value of $i$. The number of states at the inner minimum $N^{\dagger 1}_{EJ,i}$ and at the maximum $N^{\max}_{EJ,i}$ was explicitly calculated only for $J = 3$, to save computational time. The values of $N^{\dagger 1}_{EJ,i}$ and $N^{\max}_{EJ,i}$ for other values of $J = J'$ were estimated as the product of the $J = 3$ value with the factor $[(2J' + 1)/(2J + 1)]^2$, which is the ratio of the number of states at the two different $J$'s for a spherical top. From some approximate calculations, we estimate the error to be $\sim 15\%$ in the $J$-interval of greatest importance ($J = 1$ to 5). The quantities $N^{\dagger 1}_{EJ,i}$ and $N^{\dagger \max}_{EJ,i}$ were further multiplied by a quantum correction factor of 1/0.85. This latter factor corresponds to a typical average ratio of the quantum PST number of states to the "classical" PST number of states (where only the rotors are treated classically) for the values of $J$ of importance here. This quantum correction factor was included to make the evaluation of the $N^{\dagger 1}_{EJ,i}$, $N^{\dagger 2}_{EJ,i}$, and $N^{\max}_{EJ,i}$ internally consistent.

The RRKM-based vibrational probabilities used in the calculations were determined by first calculating the various vibrational number of states at about ten different energies (for each vibrational state of interest) and then using linear interpolations to determine the vibrational probabilities at any particular energy. This procedure reduced the total amount of computation involved by reducing drastically the number of energies at which the vibrational probabilities must be calculated. It also smoothed the fluctuations that arise from the Monte Carlo error bars in the calculations. The Monte Carlo error bars were on the order of 5%.

The dissociation quantum yield of a particular rotational-vibrational-electronic state of the products can be written as the product of the electronic state quantum yield and a conditional rotational-vibrational state quantum yield for the quantum state $(i,t)$ of the product, where $i$ denotes the specified quantum state of the conserved modes and $t$ a specified quantum state of one or more of the transitional modes. For example, in Table I, given later, and in the figures presented below, $i$ denotes the ground vibrational state of CO and of $^1CH_2$, apart from the specific excited $v$ states of $^1CH_2$ mentioned there, and $t$ denotes a particular value of $J$, $K_a$, and $K_c$ for the $CH_2$ group. The above conditional rota-

tional-vibrational yield is written as the product of a vibrational quantum yield $N^{eff}_{EJ,i}/\Sigma_i N^{eff}_{EJ,i}$ for state $i$ of the given electronic state, and a conditional rotational quantum yield $N^{PST}_{EJ,it}/\Sigma_t N^{PST}_{EJ,it}$. (In adopting the latter expression, we have tacitly used, as discussed at the end of the present subsection, the dynamical assumption mentioned earlier for the transitional modes.) Here, $N^{PST}_{EJ,it}$ is the PST-calculated number of states for the specified value of $i$ and $t$, and $N^{eff}_{EJ,i}$ is given by Eq. (2) when the RRKM-based calculation of the $i$ vibrational population is used. For comparison, the purely PST results are given later, in which the $N^{eff}_{EJ,i}$ of Eq. (2) is replaced by $N^{PST}_{EJ,i}$. (Thereby, PST constitutes a limiting form of Eq. (2) in which for all $i$, $N^{\dagger 1}_{EJ,i}$ and, hence, $N^{max}_{EJ,i}$, appreciably exceed $N^{\dagger 2}_{EJ,i}$.) For further comparison, the case where the $N^{eff}_{EJ,i}$ is replaced by the smaller of $N^{\dagger 1}_{EJ,i}$ and $N^{\dagger 2}_{EJ,i}$, i.e., where Eq. (1) is used, is also given later.

Finally, in concluding this section we recall, for completeness, the principal ideas involved in calculating the products' quantum state distribution.[1,4(a),8] The conservative degrees of freedom, namely the high-frequency modes, were treated adiabatically in the inner TS region and beyond. Thereby, their quantum numbers $i$ remained constant in that region, although their energy $E_i$ could vary with position along the reaction coordinate $R$ because the parameters for those vibrational modes (e.g., harmonic and anharmonic force constants) could vary along the reaction coordinate. The remaining degrees of freedom, the transitional modes, were treated "nonadiabatically," i.e., their quantum numbers were not held constant in the inner TS region and beyond to the PST TS region.

If $E$ is the total energy and $E - E_i(R)$ is the energy shared by the transitional modes, including the reaction coordinate, no constraints, other than having a total energy $E - E_i(R)$ and constant total angular momentum and $z$-component, were placed on the distribution of energy among these modes at any value $R$ of the reaction coordinate between the two transition states. In this way the distribution of orbital angular momenta at the outer transition state was, *given* an $i$ distribution fixed at $R^{\dagger 1}_{EJ,i}$, that appropriate to PST. It then followed that at subvibrational excitation energies of products, the products' quantum state distribution was that predicted by PST.[8] At higher energies, for any given excitation $i$ of the products' vibrational modes, the resulting products' quantum state *conditional* distribution for the transitional modes was the same as PST, since the latter also allows ready redistribution of energy among all transitional modes (indeed, among all modes) up to the PST region. The only difference from PST, and it is often a large one, is in the distribution of the $i$'s, the excited products' vibrational states, since in PST the latter is determined only at the PST TS, while in the present description it is determined instead from the $N^{eff}_{EJ,i}$ appearing in Eq. (2), namely from the ratio $N^{eff}_{EJ,i}/\Sigma_i N^{eff}_{EJ,i}$. It will also sometimes happen that a channel $i$ that is open at $R^{\dagger 1}_{EJ,i}$ ($N^{\dagger 1}_{EJ,i} > 0$) is closed in the PST TS region ($N^{\dagger 2}_{EJ,i} = 0$) or, much more rarely, the reverse ($N^{\dagger 2}_{EJ,i} = 0$, $N^{\dagger 1}_{EJ,i} > 0$). In either case, as one sees from Eq. (2), $N^{eff}_{EJ,i}$ is dominated by the lesser of these and so vanishes in each of these cases, and so the channel is closed.

### B. PHOFEX spectra

In the PHOFEX spectra[9-11] for the $^1CH_2CO$ dissociation, the dependence on energy of the yield of a particular vibrational-rotational state of the $CH_2$ fragment is probed. The determination of a theoretical PHOFEX spectrum for subvibrational excess energies was described by Moore and co-workers.[9,10] They noted that a theoretical calculation involves (1) the determination of the distribution of initial ketene vibrational-rotational states, (2) the determination of the rotational line strengths for the ketene photoexcitation process, and (3) the determination of the dissociation quantum yields at given fixed total energies and total angular momenta for the $CH_2$ rotational-electronic state of interest.

At excess energies exceeding the threshold for vibrational excitation of the products,[10] the vibrational part of the dissociation quantum yield must also be considered. The above definition of the rotational-vibrational-electronic state quantum yield implies that the only difference between the calculation of PHOFEX spectra using PST-based and the RRKM-based theory of Ref. 8 is in their vibrational quantum yields. Additionally, this separation into rotational, vibrational, and electronic factors allows us to use *quantum* PST for the rotational distribution (even in the RRKM-based calculations) and thereby to reproduce the steps that occur in the PHOFEX spectra when each new CO rotational channel becomes open.

In summary, the method used for determining the predicted PHOFEX spectra is similar to that which was described in Refs. 9 and 10 for the subvibrational excitation of the products, namely PST-based calculations of the numbers of available states are still used for the rotational distribution, but now the definition of the quantum yield is modified to include a calculation of the vibrational part, using Eq. (2) or, for comparison, Eq. (1) or the PST result. Also, since the excess energies for vibrational excitations are quite large, the triplet rate constant may be considered to be quite small relative to the singlet rate constant.[9,10] This conclusion implies that the singlet quantum yield for those states should be near unity and therefore should not vary too strongly with energy. Thus, in the present calculations for excess energies exceeding the threshold for vibrational excitation, the singlet quantum yield has been set equal to unity. This assumption can be re-examined when more experimental data become available. For the ground vibrational state, needed for Table I, the triple yield was assumed to be that which was determined by the "fit" of the triplet number of states to the experimental spectrum, described in Ref. 9.

In the work of Moore and co-workers, the dependence of the number of $^1CH_2$ molecules produced in a particular vibrational-rotational state, as a function of the excess energy, was determined via a measurement of the intensity of the laser induced fluorescence (LIF) of the specific rotational state of $^1CH_2$ as a function of the photolysis laser wavelength. The ratio of this LIF intensity to the laser photolysis power (and, when the transitions are not saturated, divided by the probe laser power also) then provided a "signal intensity" which, when plotted against wavelength, can be termed a PHOFEX spectrum.

Two PHOFEX spectra (one spectrum for the ground vibrational state, and one for the vibrationally-excited state of interest) may be used to compare theory and experiment in several ways. One direct route for comparing values of this ratio involves a comparison of the theoretically-calculated ratio of the two PHOFEX spectra (including the thermal averaging over the initial distribution of ketene states) at specified wavelengths with the corresponding experimental ratio, taking into account the difference in intrinsic LIF intensities of $CH_2$ from the two rovibrational states. While these ratios can be quite easily determined for the PST and the two RRKM-based calculations, the corresponding experimental ratios are not easily obtained. At present, the only state for which Moore and co-workers have experimentally determined a ratio of rovibrational populations is the $J_{K_a,K_c} = 1_{01}$ rotational state of the $v = 1$ HCH bending vibration,[11] relative to that rotational state in the ground vibrational state: More specifically, the ratio of the signal intensity for this state at a photolysis wavelength of 316.809 nm to that for the same rotational state of the ground vibrational state at a photolysis wavelength of 330.039 nm, was determined[11] after taking into account various correction factors associated with the measurement techniques, including one mentioned above. The value of this ratio was[11] 0.075 and is listed later in Table I.

Alternatively, the experimental signal intensity ratios have been used to give an estimated vibrational quantum yield in a different way:[11] The quantum yield for a given initial ketene state may be written as a product of an electronic state quantum yield and of conditional probabilities for the rotational and vibrational quantum yields, as described earlier. Any thermal distribution of the initial ketene states then necessitates a convolution of the above three factors. However, if it is assumed that this thermal averaging has a measurable effect only on the rotational quantum yields, one may use the PST-estimated rotational quantum yields (including the thermal averaging) together with the experimentally estimated electronic quantum yields to obtain from the data an estimated "experimental" vibrational quantum yield. This estimate is, of course, predicated on the assumption of the validity of PST for the calculation of the conditional rotational quantum yields, as well as on the neglect of the thermal averaging for the vibrational and electronic quantum yields. For the particular case of the HCH bending vibration, at an excess energy of 1500 $cm^{-1}$, the vibrational excitation probability to the $v = 1$ state was estimated in this way by Moore and co-workers[11] to be 0.030. In Part I, we found that the corresponding RRKM-based vibrational excitation probabilities were 0.030 and 0.025 for calculations based on Eqs. (1) and (2), respectively, while the corresponding PST determined vibrational excitation probability[1] was appreciably smaller, 0.0089.

A third comparison of theory and experiment, in the absence of a knowledge of the absolute LIF intensities for the other states of $CH_2$, is to scale the experimental results, each figure given later having its own scaling factor, and compare the shapes of the plots. We have done this in those figures by making the RRKM-based Eq. (2) expression agree with the experimental results at the latter's maximum or asymptote. We have also used a similar procedure, in which, instead, the scaling was such that the PST results agreed with the experimental ones near the maximum in the latter. A typical example of the latter PST-scaled result is given later in Fig. 7, for the same state considered in Fig. 2. PST-scaled plots for the other states are not shown but their appearance is largely similar and we comment on them in the next section.

## III. RESULTS AND DISCUSSION

In Table I, the theoretically-calculated ratios of signal intensities are given for all the vibrational states to be considered. From the results in Table I it is seen that, for all of the vibrational-rotational states considered, the RRKM-based results for the ratio of signal intensities are significantly greater than the PST results. The finding that the PST-calculated vibrational probability is too low (first line, Table I) agrees with previous experimental results[18] for NCNO. For the latter, the RRKM-based calculations again showed closer agreement.[6] In Figs. 1–6, the results of the RRKM-based theory calculations and the PST calculations of the PHOFEX spectra are plotted, together with the experimentally determined spectra of Moore and co-workers,[11] scaled to

TABLE I. Ratio of signal intensity of vibrationally-excited photofragment excitation spectra to that for the $1_{01}$ rotational state of the ground vibrational state of $CH_2$ at an excess energy of 183.25 $cm^{-1}$.

| $CH_2$ Vibrational State | $CH_2$ Rotational State ($J_{K_a,K_c}$) | Excess Energy ($cm^{-1}$) | Ratios RRKM [Eq. (1)] | RRKM [Eq. (2)] | PST | EXPT |
|---|---|---|---|---|---|---|
| $v_{HCH} = 1$ | $1_{01}$ | 1448.5[a] | 0.080 | 0.055 | 0.016 | 0.075 |
| $v_{HCH} = 1$ | $2_{02}$ | 1618.5 | 8.3 | 6.8 | 3.4 | — |
| $v_{HCH} = 1$ | $3_{03}$ | 1702 | 0.087 | 0.081 | 0.050 | — |
| $v_{HCH} = 1$ | $3_{21}$ | 1720 | 0.075 | 0.070 | 0.041 | — |
| $v_{HCH} = 2$ | $1_{01}$ | 2890 | 0.021 | 0.015 | 0.0051 | — |
| $v_{CH}^{sym} = 1$ | $1_{01}$ | 2953 | 0.013 | 0.010 | 0.0038 | — |

[a] The energy at which the ratio for the $v_{HCH} = 1$, $J_{K_a,K_c} = 1_{01}$ state has been determined corresponds to the energy at which the experimental ratio of 0.075 was determined. All other energies in this column correspond to the energy at which the maximum occurs in the vibrationally-excited photofragment excitation spectrum for the RRKM-based calculation that uses Eq. (2).

agree with the results for Eq. (2) near the maximum.[19]

The plot based on Eq. (2) is seen in Figs. 1–6 to have a shape for the energy dependence that agrees better than does that based on Eq. (1). It shows a fairly rapid rise in intensity from the threshold to about 100 $cm^{-1}$ excess energy, followed by a region of nearly constant intensity. The difference observed here between the RRKM-based treatment based on a single minimum in $N^{\dagger}_{EJ,i}$, Eq. (1), and, that based on Eq. (2), is seen in the figures to exist only in the region centered about 100 $cm^{-1}$ above each vibrational excitation threshold. This energy region corresponds to the region where the lowest of the two minima in the number of states plot changes from being the outer minimum to the inner one. The treatment based on Eq. (1) alone yields too sudden a change in the derivative of the number of states with respect to energy accompanying this change of the minimum, as is evident in plots based on Eq. (1) in Figs. 1–6. Instead, in the treatment based on Eq. (2) this change in slope is smoothed over an interval of about 100 $cm^{-1}$, so matching more closely the experimental results. The greatest discrepancies between the RRKM-based Eq. (2) treatment and the experimental data arise in Figs. 3 and 4, where the energy scan lengths are somewhat longer than in the others.

We have also explored, as already noted, a comparison analogous to Figs. 1–6, but where the PST results were scaled to agree near the experimental maximum or asymptote. For such plots, the counterparts of Figs. 1–3, 5,6 showed relatively poor agreement (only that for Fig. 4 showed reasonable agreement), the PST results continuing to rise even after the experimental results have reached a maximum or an asymptote. A typical example is given in Fig. 7.

The principal difference between the shape of the three plots in Figs. 1–6 (seen for PST most clearly when the latter is scaled to the experimental results, as in Fig. 7) is that the PST value uses $N^{\dagger 2}_{EJ,i}$ for $N^{eff}_{EJ,i}$ at all energies and for all values of $i$ in a plot. This use of $N^{\dagger 2}_{EJ,i}$ results in two errors in the PST plots: (1) in the PST expression for the vibrational probability, given by $N^{\dagger 2}_{EJ,i}/\Sigma_i N^{\dagger 2}_{EJ,i}$, the denominator tends to be much too large and hence the initial slope too small; (2) if the PST denominator is scaled to yield agreement at the threshold (where a scaled result is expected to fit best since $N^{\dagger 2}_{EJ,i} < N^{\dagger 1}_{EJ,i}$ there), much too high an intensity is obtained at the higher energies in a PHOFEX plot. Again the Eq. (1)-based plot jumps sharply from the case where $N^{\dagger 2}_{EJ,i}$ is dominant (energies near the threshold) to that where $N^{\dagger 1}_{EJ,i}$ is dominant (higher energies). Only the Eq. (2)-based plot goes smoothly from an $N^{\dagger 2}_{EJ,i}$-dominated region near threshold to an $N^{\dagger 1}_{EJ,i}$-dominated one as the energy in a PHO-

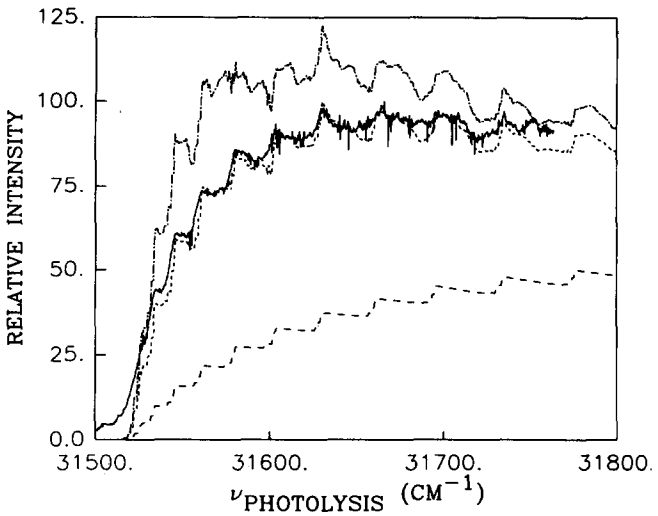


FIG. 2. Same as for Fig. 1, but for the $v_{HCH} = 1$, $J_{K_a K_c} = 2_{02}$ vibrational-rotational state of methylene. The excess energy ranges from approximately 1385 $cm^{-1}$ to 1685 $cm^{-1}$.

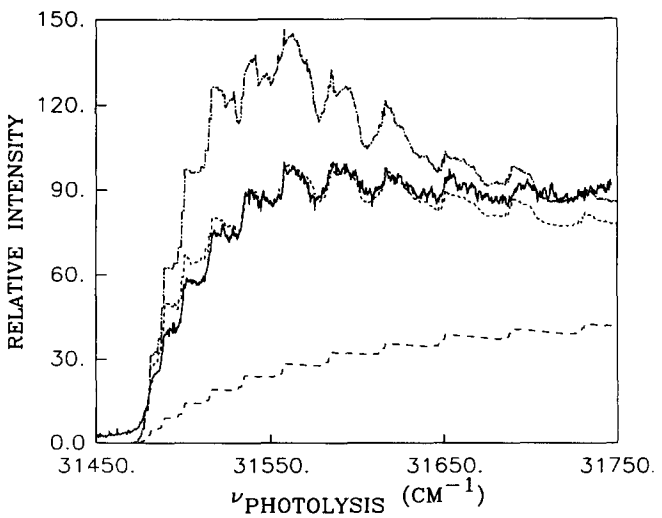


FIG. 1. Photofragment excitation spectrum for the $v_{HCH} = 1$, $J_{K_a K_c} = 1_{01}$ vibrational-rotational state of methylene. The experimental results are given by the solid line, the PST results by the long-dashed line (the lowest line), the absolute minimum RRKM-based results [cf. Eq. (1)] by the dot-dashed lines (highest line), and the RRKM-based treatment based on Eq. (2) by the short dashed line (the line which most closely follows the experimental trend). The excess energy ranges from approximately 1335 $cm^{-1}$ to 1635 $cm^{-1}$.

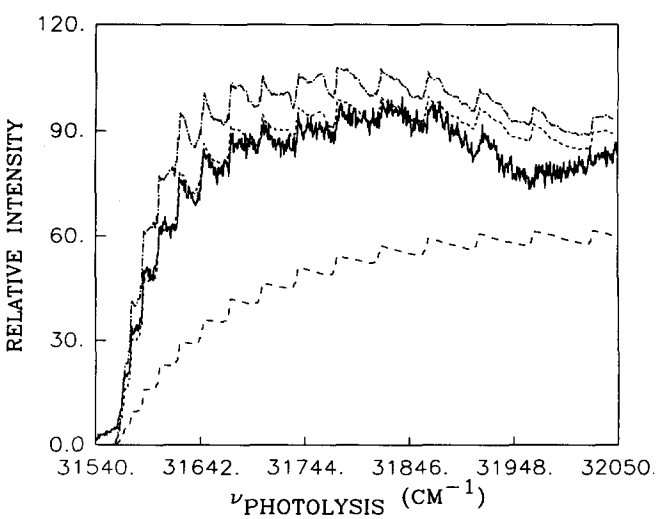


FIG. 3. Same as for Fig. 1, but for the $v_{HCH} = 1$, $J_{K_a K_c} = 3_{03}$ vibrational-rotational state of methylene. The excess energy ranges from approximately 1425 $cm^{-1}$ to 1935 $cm^{-1}$.

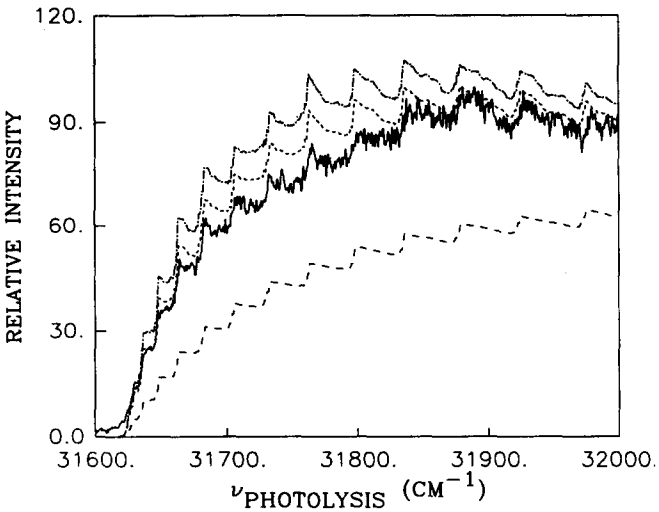


FIG. 4. Same as for Fig. 1, but for the $v_{HCH} = 1$, $J_{K_aK_c} = 3_{21}$ vibrational-rotational state of methylene. The excess energy ranges from approximately 1485 $cm^{-1}$ to 1885 $cm^{-1}$.

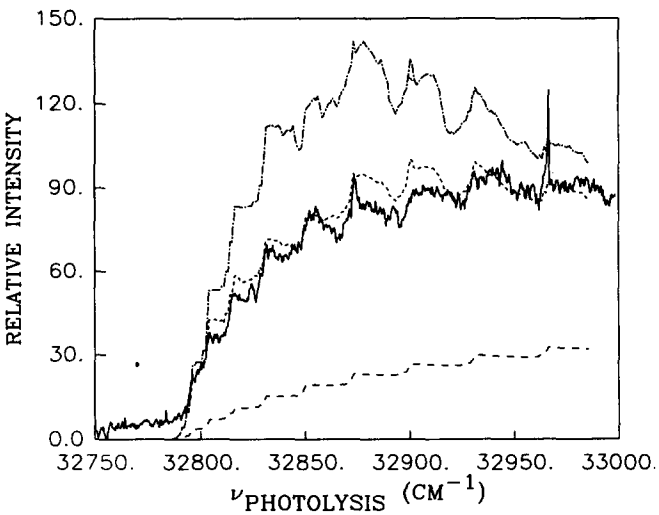


FIG. 5. Same as for Fig. 1, but for the $v_{HCH} = 2$, $J_{K_aK_c} = 1_{01}$ vibrational-rotational state of methylene. The excess energy ranges from approximately 2635 $cm^{-1}$ to 2885 $cm^{-1}$.

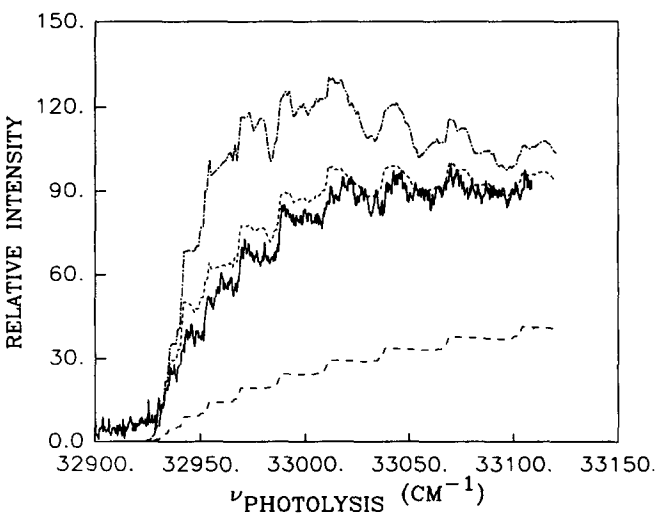


FIG. 6. Same as for Fig. 1, but for the $v_{CH}^{sym} = 1$, $J_{K_aK_c} = 1_{01}$ vibrational-rotational state of methylene. The excess energy ranges from approximately 2785 $cm^{-1}$ to 3035 $cm^{-1}$.

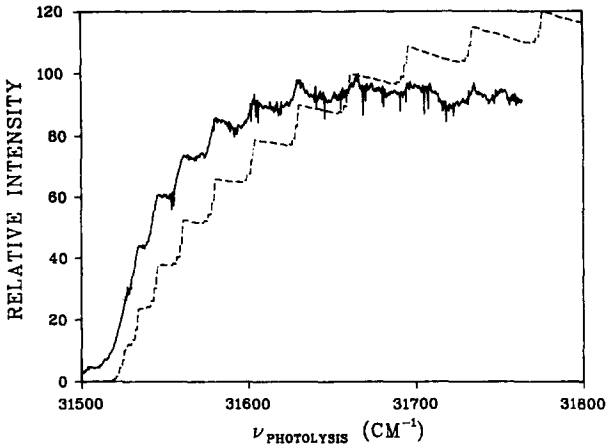


FIG. 7. Same as for Fig. 2, but showing only the experimental curve (solid curve) and the PST results (dashed curve) scaled to agree with the experimental near a maximum in the latter.

FEX plot is increased. This shift of the transition state from one in the PST region at the threshold of the $i$-excitation to one in the inner region at $R^{\dagger}_{EJ,i}$ at higher energies in the PHOFEX plot is a principal feature in the present calculation. The results in Figs. 1–6 indicate a convergence of the plots based on Eqs. (1) and (2) when the excess energy is at least $\sim 200$ $cm^{-1}$ above each vibrational threshold, since the effect of $N^{\dagger 1}_{EJ,i}$ is dominant there (i.e., $N^{\dagger 1}_{EJ,i} < N^{\dagger 2}_{EJ,i}$).

At lower excess energies, the important role of $R^{\dagger}_2$ is clear from such figures. The staircase nature of the plots in that region reflects the quantum nature of the PST calculation of the transitional modes at $R^{\dagger}_2$ in both Eq. (1) and Eq. (2). For $J_{K_aK_c} = 1_{01}$ (e.g., in Figs. 1, 5, and 6) at threshold there is only one product $^1CH_2$ rotational state accessible for the given vibrational state, namely $1_{01}$.[11] Thus the conditional quantum yield of the $1_{01}$ rotational quantum state of $^1CH_2$ (conditional, given the vibrational and electronic state of $CH_2$ and CO) is unity until the next $CH_2$ rotational state of the same spin, initially $1_{10}$, is accessible ($\sim 15$ $cm^{-1}$ higher in energy). When that state becomes accessible the conditional rotational quantum yield of the $1_{01}$ state becomes less than unity, an effect taken into account in the present calculation. It has been noted in Ref. 11 that the spacing of the steps in Figs. 1, 5, and 6 corresponds to that of the rotational energy levels of isolated CO, thereby suggesting the importance of a very loose transition state (i.e, $R^{\dagger}_2$) at threshold. A similar result also holds for the threshold of the para spin state[11] $J_{K_aK_c} = 0_{00}$, although no results are shown in the present paper for this state.

While the agreement with Eq. (2) on the shape of the energy-dependence in these figures may be in some sense better than might have been expected, due to the model nature of the potential energy surfaces used here, some small changes of parameter values in this model surface did not change the qualitative picture seen in Fig. 1. Although the results for the spectra given in Figs. 1–6 are encouraging, it would be especially useful to supplement the absolute experimental signal intensity for the $1_{01}$ $v_{HCH} = 1$ state by those of the other states.

If the calculation of interest had been one of microcanonical rate constants $k_{EJ}$, as it was in part in Part I, rather than of production of individual quantum states, Eq. (1), rather than Eq. (2), averaged over all states $i$ to obtain an $R^{\dagger}_{EJ}$, would have largely sufficed. In such a calculation in Part I, the conserved mode states whose threshold happens to be close to $E$ contribute relatively little to $k_{EJ}$, except in the immediate threshold of $k_{EJ}$ itself, because of the large contribution to $k_{EJ}$ from $i$ states not near their thresholds. Thereby, except at the $k_{EJ}$ threshold, the counterpart of Eq. (2) for an $N_{EJ}(R)$ yields essentially the same result as that of Eq. (1), as was found in Part I and in Ref. 6.

## IV. SUMMARY

A principal feature of the present treatment of the excitation of a vibrational state, observed in a PHOFEX spectrum, is the two-transition state nature for the excitation, the PST region dominating just above the particular excitation and the inner TS region dominating at somewhat higher excess energies ($\sim 200\,\mathrm{cm}^{-1}$ for the present system). According to the present analysis and results, neither the PST nor the Eq. (1)-based treatment is as satisfactory as the composite treatment based on Eq. (2), in terms of consistency and of current agreement with experimental data. For calculations of $k_{EJ}$ itself, use of the counterpart of a single TS Eq. (1) was satisfactory, except at the threshold of $k_{EJ}$, as discussed at the end of the preceding section.

## ACKNOWLEDGMENTS

It is a pleasure to acknowledge the support of this research by the National Science Foundation. The authors would also like to thank W. H. Green, Jr., A. J. Mahoney, C.-k. Cheng, and C. B. Moore for making the results of their photofragment excitation spectra available to us prior to publication, and for their collaboration in the comparison of the experimental and theoretical photofragment excitation spectra.

[1] S. J. Klippenstein and R. A. Marcus, J. Chem. Phys. **91**, 2280 (1989) (hereinafter referred to as Part I).

[2] E. D. Potter, M. Gruebele, L. R. Khundkar, and A. H. Zewail, Chem. Phys. Lett. **164**, 463 (1989).

[3] P. Pechukas and J. C Light, J. Chem. Phys. **42**, 3281 (1965); P. Pechukas, R. Rankin, and J. C. Light, J. Chem. Phys. **44**, 794 (1966); C. Klotz, J. Phys. Chem. **75**, 1526 (1971).

[4] (a) R. A. Marcus, Phil. Trans. Roy. Soc. A (in press). (b) This trend for PST with $T$ is discussed, for example, in Ref. 4(a) and by Rai and Truhlar, Ref. 7. With most other treatments, this trend of inward movement of the transition state with increasing $T$ frequently leads to a corresponding decrease of the rate constant $k_{bi}(T)$ for fragment recombination (Refs. 5–7). However, for PST the effect of this movement is so small, for a long range attractive $R^{-6}$ potential between the fragments, and since there are no concomitant increased steric effects in PST, the tendency for $k_{bi}(T)$ to decrease is overcome by the positive $T$ effect on the velocity-weighted rate of crossing the barrier [Ref. 4(a)].

[5] D. M. Wardlaw and R. A. Marcus, Chem. Phys. Lett. **110**, 230 (1984); D. M. Wardlaw and R. A. Marcus, J. Chem. Phys. **83**, 3462 (1985); D. M. Wardlaw and R. A. Marcus, J. Phys. Chem. **90**, 5383 (1986); D. M. Wardlaw and R. A. Marcus, Adv. Chem. Phys. **70**, 231 (1988), and references cited therein.

[6] S. J. Klippenstein, L. R. Khundkar, A. H. Zewail, and R. A. Marcus, J. Chem. Phys. **89**, 4761 (1988).

[7] W. L. Hase, J. Chem. Phys. **64**, 2442 (1976); M. Quack and J. Troe, Ber. Bunsenges. Phys. Chem. **81**, 329 (1977); G. P. Smith and D. M. Golden, Int. J. Chem. Kinet. **10**, 489 (1978); S. N. Rai and D. G. Truhlar, *ibid.* **79**, 6046 (1983); S. W. Benson, Can. J. Chem. **61**, 881 (1983); W. L. Hase and D. M. Wardlaw, in *Bimolecular Collisions*, edited by J. E. Baggott and M. N. Ashfold (Royal Society of Chemistry, Burlington House, London, 1989), p. 171; X. Hu and W. L. Hase, J. Phys. Chem. **93**, 6029 (1989), and references cited therein.

[8] R. A. Marcus, Chem. Phys. Lett. **144**, 208 (1988).

[9] I.-C. Chen, W. H. Green, Jr., and C. B. Moore, J. Chem. Phys. **89**, 314 (1988).

[10] W. H. Green, Jr., I.-C. Chen, and C. B. Moore, Ber. Bunsenges. Phys. Chem. **92**, 389 (1988).

[11] W. H. Green, Jr., A. J. Mahoney, C.-k. Cheng, and C. B. Moore (private communication) and J. Chem. Phys. (submitted).

[12] M. Quack and J. Troe, Ber. Bunsenges. Phys. Chem. **78**, 240 (1974); J. Troe, J. Phys. Chem. **88**, 4375 (1984), and references cited therein.

[13] I. Nadler, M. Noble, H. Reisler, and C. Wittig, J. Chem. Phys. **82**, 2608 (1985); C. X. W. Qian, M. Noble, I. Nadler, H. Reisler, and C. Wittig, J. Chem. Phys. **83**, 5573 (1985); C. Wittig, I. Nadler, H. Reisler, M. Noble, J. Catanzarite, and G. Radhakrishnan, J. Chem. Phys. **83**, 5581 (1985).

[14] S. J. Klippenstein and R. A. Marcus, J. Phys. Chem. **92**, 5412 (1988).

[15] W. H. Miller, J. Chem. Phys. **65**, 2216 (1976); J. O. Hirschfelder and E. Wigner, *ibid.* **7**, 616 (1939); W. J. Chesnavich, L. Bass, T. Su, and M. T. Bowers, *ibid.* **74**, 2228 (1981); S. N. Rai and D. G. Truhlar, *ibid.* **79**, 6046 (1983).

[16] We use, as in Ref. 1, a value of $1.8\,\text{Å}^{-1}$ for the interpolation parameters $\alpha$ (an approximation that can be avoided when the detailed potential energy surface becomes known). In addition to the comparisons with an $\alpha = 1.0\,\text{Å}^{-1}$ described in Ref. 1, the use of the latter $\alpha$ showed too slow an increase with energy for the $\upsilon_{\mathrm{HCH}} = 2$ PHOFEX spectra for the $J_{K_a K_c} = 1_{01}$ rotational state.

[17] In the case of the $C_6$ potential parameter describing the strength of the long range attractive potential, a value of $1\times 10^{20}\,\mathrm{cm}^{-1}\,\text{Å}^6$ was again used.[1] This value corresponds to having the phase space transition state effectively at $R = \infty$ and is in keeping with the finding of Moore and coworkers[9,10] (for the subvibrational PHOFEX spectra) that this parameter is constrained to be greater than $5\times 10^4\,\mathrm{cm}^{-1}\,\text{Å}^6$. Sample calculations were also performed for the latter value of $C_6$ which indicated only a very small difference (typically less than 5%) from those performed with the "infinitely loose" value.

[18] C. X. W. Qian, M. Noble, I. Nadler, H. Reisler, and C. Wittig, J. Chem. Phys. **83**, 5573 (1985), and references cited therein.

[19] In Fig. 5, the spike in the experimental data at an energy of $32970\,\mathrm{cm}^{-1}$ was assumed to be an experimental artifact and neglected in the present scaling of the experimental results in that plot.